Full Title: Highly sensitive *in vivo* detection of dynamic changes in enkephalins following acute stress

Short Title: *In vivo* detection of enkephalins during stress

Authors: Marwa O. Mikati[1,2,3], Petra Erdmann-Gilmore[4], Rose Connors[4], Sineadh M. Conway[1,2,3], Jim Malone[4], Justin Woods[1,2,3], Robert W. Sprung[4], R. Reid Townsend[4], Ream Al-Hasani* [1,2,3].

[1]Department of Anesthesiology, [2]Washington University Pain Center, Washington University in St. Louis, MO, USA; [3]Center for Clinical Pharmacology, University of Health Science and Pharmacy in St. Louis, MO, USA, [4]Department of Medicine, Washington University School of Medicine, Washington University in St. Louis, St. Louis, MO, USA

***Correspondence:** Ream Al-Hasani, PhD: al-hasanir@wustl.edu.

Abstract: Enkephalins are opioid peptides that modulate analgesia, reward, and stress. *In vivo* detection of enkephalins remains difficult due to transient and low endogenous concentrations and inherent sequence similarity. To begin to address this we previously developed a system combining in vivo optogenetics with microdialysis and a highly sensitive mass spectrometry-based assay to measure opioid peptide release in freely moving rodents (Al-Hasani, 2018, eLife). Here we show improved detection resolution and stabilization of enkephalin detection, which allowed us to investigate enkephalin release during acute stress. We present an analytical method for real-time, simultaneous detection of Met- and Leu-Enkephalin (Met-Enk & Leu-Enk) in the mouse Nucleus Accumbens shell (NAcSh) after acute stress. We confirm that acute stress activates enkephalinergic neurons in the NAcSh using fiber photometry and that this leads to the release of Met- and Leu-Enk. We also demonstrate the dynamics of Met- and Leu-Enk release as well as how they correlate to one another in the ventral NAc shell, which was previously difficult due to the use of approaches that relied on mRNA transcript levels rather than post-translational products. This approach increases spatiotemporal resolution, optimizes the detection of Met-Enkephalin through methionine oxidation, and provides novel insight into the relationship between Met- and Leu-Enkephalin following stress.

Introduction

Endogenous opioid peptides are released at significantly lower concentrations than small molecule neurotransmitters and undergo post-translational processing that yields ~30 unique peptides from 4 precursor molecules. Together, these properties have made sensitive peptide detection difficult to achieve with existing technologies [1]. Here, we describe an analytical method that enables quantification of dynamic *in vivo* changes in both Leu- and Met-enkephalin (Leu-Enk and Met-Enk) peptides in rodents. We show unique release profiles between Leu- and Met-Enk in response to two different stressors and gain new insight into peptide release dynamics; additionally, our method offers improved spatiotemporal resolution. More broadly, this approach

will enable an understanding of how neuropeptide levels change in response to acute or chronic behavioral, pharmacological, and neurophysiological manipulations.

Enkephalins can act on both the delta and/or mu opioid receptors, but their activity often depends on receptor and peptide expression patterns, which differ across the brain [2–5]. Confirming an opioid peptide's identity based on the activity of the receptor alone poses difficulties. For example, in a single brain region, the mu opioid receptor may be activated by an enkephalin or endorphin peptide [3]. Therefore, any technique that relies on a readout of mu opioid receptor activity is not sufficient to determine whether the peptide is an endorphin or an enkephalin. It has been particularly challenging to measure Met- and Leu-Enk selectively and independently *in vivo*; in fact, both peptides are typically referred to as 'enkephalins', which oversimplifies their distinct properties. Though antibody-based techniques [6–9] or liquid chromatography/mass spectrometry (LC-MS) [10–12] have improved Met- and Leu-Enk detection somewhat, limitations such as spatiotemporal restrictions and poor selectivity between enkephalins remain. Our group previously developed real-time *in vivo* detection of evoked opioid peptide release using microdialysis/nanoLC-MS (nLC-MS) after photostimulation [13]. From this strong foundation, we have now optimized a novel opioid peptide detection technique. For the first time, we can selectively measure real-time *in vivo* levels of basal (non-evoked) peptide release, as well as during behavioral manipulations. Our primary goals in establishing this analytical workflow to measure opioid peptide dynamics *in vivo* were to 1) increase temporal resolution allowing for the detection of dynamic changes to short external stimuli and acute conditions, 2) lower the detection threshold to allow for accurate measurements from small brain regions using less volume of sample, 3) measure endogenous release of peptides in the native state without the need for photo- or chemogenetic stimulation, 4) report raw values of measured concentrations rather than % baseline measurements, 5) enable real-time, simultaneous detection of both Met- and Leu-Enk. To meet these goals and measure both Leu- and Met-Enk we used an improved and specialized microdialysis technique coupled with nLC-MS.

Results

Optimizing a method for the simultaneous *in vivo* detection of Met- and Leu-Enkephalin

Our workflow (**Fig. 1A**) starts with stereotaxic surgery to implant the microdialysis probe in the mouse nucleus accumbens shell (NAcSh). Along with others, we have shown that the opioid receptor system in the NAcSh mediates both reward and aversion through photostimulation of peptide-expressing neurons across the dorsal/ventral axis [14–20]. Our aim was to measure NAcSh peptide release in response to aversive, stressful stimuli. We use custom-made microdialysis probes, intentionally modified so they are similar in size to commonly used fiber photometry probes thus causing comparable levels of tissue damage (**Fig. 1B**). Importantly, the membrane that sits above the brain region of interest is smaller in diameter when compared to a photometry probe (**Fig. 1B**). After recovery, we begin microdialysis collection every 13 minutes, circulating artificial cerebrospinal fluid (aCSF) and collecting interstitial fluid (ISF) at a flow rate of 0.8 μL/min. After each sample collection, we add a consistent known concentration of isotopically labeled internal standard of Met-Enk and Leu-Enk of 40 amol/sample to the collected ISF for the accurate identification and quantification of endogenous peptide. These internal standards have a different mass/charge (m/z) ratio than endogenous Met- and Leu-Enk. Thus, we can identify true endogenous signal for Met-Enk and Leu-Enk (**Suppl Fig. 1A,C**) versus noise, interfering signals, and standard signal (**Suppl. Fig. 1B,D**). Importantly, we have resolved one of the main barriers preventing the accurate quantification of Met-Enk: the variable oxidation of the methionine residue during sample processing, which results in the signal for Met-Enk being split among multiple m/z values thereby impairing sensitivity. In order to ensure that the signal for Met-Enk is represented by a single m/z value, we converted all methionyl residues to the doubly oxidized sulfone prior to nLC-MS analysis, which allows us to reliably quantify Met-Enk and differentiate it from Leu-Enk without compromising the detection of either peptide [21]. Beyond opioid peptides, this approach represents a key advance and can be applied to any peptide containing a

95 methionine residue. As seen in **Fig. 1C.**, before the methionine oxidation reaction at time 0, Met-
96 Enk can be observed in unoxidized, and singly- and doubly-oxidized forms with varying intensities.
97 However, after the reaction is complete at time 1, Met-Enk is observed as doubly oxidized with
98 much higher intensity enabling accurate quantification.
99 To increase the signal to noise ratio, we also performed solid-phase extraction after the oxidation
100 reaction which removes any salt from the collected samples. To determine the lower limit of
101 quantification (LLOQ), forward and reverse curves were created using varying concentrations of
102 the Met- and Leu-Enk standards in accordance with Clinical Proteomics Tumor Analysis
103 Consortium (CPTAC) guidelines [22]. We determined that the lower limit of quantification (LLOQ),
104 for both Leu-Enk and Met-Enk is 40 amol/sample (**Fig. 1D-E**). The improved quantification limit
105 means increased temporal resolution. We now need less volume, (10 μL or less), and shorter
106 sampling times: 10 minutes or less, rather than 15-20 minutes as compared to previous studies
107 [13,23]. To test the utility of the method in measuring real-time changes in peptide levels *in vivo*,
108 we evoked the release of the peptides using high K^+ ringer's solution, which depolarizes the cells
109 and causes the release of dense core vesicles containing neuropeptides [24]. This depolarization
110 state significantly increased the release of Met- and Leu-Enk in the NAcSh as compared to
111 baseline **Fig.1F**. Interestingly, Leu-Enk showed a greater fold change compared to baseline than
112 did Met-Enk with the fold changes being 28 and 7 respectively based on the data in **Fig.1F**.
113 Previous studies reporting opioid peptide measurements rarely represent raw concentrations
114 measured. Instead, most past studies reported changes in peptide concentrations as % of
115 baseline [10,13,23]. One key advantage of our improved method is that we can detect reliable
116 measurements of both Met- and Leu-Enk at baseline reported as concentrations in the
117 amol/sample range. We then quantified the ratio of the Met- to Leu-Enk after applying high K+
118 solution and showed that this ratio is 3:1 in the NAcSh (**Fig. 1G-H**). The release of Met-Enk is
119 postulated both in vitro and ex vivo to be between 3 to 4 times that of Leu-Enk [25–27]. We are
120 the first to not only corroborate the predicted ratio *in vivo* in freely behaving animals, but

121 specifically in the NAcSh. Interestingly, this 3:1 ratio is almost identical to that previously reported
122 in homogenized human tissue from the sympathoadrenal systems using radioimmunoassays [28].
123 Importantly, this conserved ratio highlights the usefulness of rodent models for investigating the
124 highly conserved opioid system and demonstrates its potential in translation to humans.

125 **Experimenter handling drives the release of Met- and Leu-Enkephalins in the NAcSh**

126 To highlight the applicability and value of this improved approach, we investigated the changes
127 in the levels of enkephalins following acute stress. It has been hypothesized that enkephalins act
128 as anti-stress signals based on studies that have shown increased preproenkephalin transcript
129 levels following acute stress [29–32]. These studies have included regions such as the locus
130 coeruleus, the ventral medulla, the basolateral nucleus of the amygdala, and the nucleus
131 accumbens core and shell. Studies using global knockout of enkephalins have shown varying
132 responses to chronic stress interventions where male knockout mice showed resistance to
133 chronic mild stress in one study, while another study showed that enkephalin-knockout mice
134 showed delayed termination of corticosteroid release. [33,34]. Moreover, decreased enkephalin
135 expression in the NAc was correlated with an increase in the susceptibility to social defeat [35].
136 This body of literature supports the hypothesis that enkephalins participate in stress encoding and
137 reactivity. We were specifically interested in how enkephalins mediate acute stress responses.
138 Our group has also recently demonstrated that the photostimulation of a subpopulation of
139 peptidergic neurons in the NAcSh drives aversion [14], which further suggests a role for neurons
140 in the NAcSh during aversive stimuli such as stress. Despite the wealth of data implicating these
141 peptides in the stress response, it has not been possible to measure the dynamics of real-time
142 peptide release in response to acute stressful stimuli. We sought to test the hypothesis that Met-
143 and Leu-Enk are released in the NAcSh following acute stress. Using the nLC-MS detection
144 method, we successfully monitored dynamic changes of Met- and Leu-Enk during two different
145 stressors. The first stressor was defined as experimenter handling, which involves the

146 experimenter scruffing the mouse while connecting to the dialysis set up (**Fig. 1A**). The second
147 stressor was exposure to predator odor (i.e., fox urine).
148
149 We show that both Met- and Leu-Enk are released following experimenter handling, and that the
150 levels decrease within minutes after exposure to the stress (**Fig. 2A**). We also analyzed the data
151 with sex as a main effect and did not find any differences between males and females after
152 correcting for multiple comparisons (**suppl. Fig. 2A**). We corroborate our finding from **Fig. 1G-H**
153 showing that the ratio of 3:1 Met-Enk to Leu-Enk is conserved following experimenter handling
154 (**Fig. 2C**). Another key finding is that peptide release appears to be precisely controlled. We show
155 that the amol/sample of Met-Enk released at the beginning of the experiment is predictive of later
156 release. For example, a higher level released (in the fmol/sample range) during the first collections
157 results in lower levels released (in the amol/sample range) during later collections and vice versa
158 (**Fig. 2D**). We show a negative correlation (~ -0.3) between the first two samples (~26 minutes)
159 and the later timepoints, samples 3-10 (~104 minutes). Importantly, this relationship is not due to
160 Met-Enk depletion as the circulation of high K+ aCSF is sufficient to drive the release of Met-Enk
161 at the end of an experiment and reverse the negative correlation (**Fig. 2E**).
162
163 To test whether our findings regarding peptide release correlated with neuronal activity following
164 the same stressor, we also monitored enkephalinergic neuron activity using fiber photometry
165 following experimenter handling. To do this, we stereotaxically injected a Cre-dependent adeno-
166 associated virus containing the calcium sensor GCaMP6s in the NAcSh of preproEnkephalin-Cre
167 (pEnk-Cre) mice and implanted fiber photometry probes (**Fig. 2F**). During handling, we observed
168 increased calcium activity in enkephalinergic neurons, even after it was repeated twice within a
169 few minutes (**Fig. 2G**). Individual responses to experimenter handling varied appreciably, as
170 shown by the heatmaps and bar plots (**Fig. 2H-I**); such variation could be due to slight differences
171 in probe placement (**Suppl. Fig 3B,D**) as peptidergic neurons in the dNAcSh encode reward while

172 neurons in the vNAcSh encode aversion [14,36]. Furthermore, the enkephalin precursor is
173 expressed across the dorsal-ventral axis as shown in the *in situ* hybridization atlas (Allen Brain
174 Institute). The fiber photometry data and peptide release data are concordant, as enkephalinergic
175 neurons are activated following experimenter handling, which drives Met- and Leu-Enk
176 somatodendritic release. However, the photometry and peptide release data differ in that repeated
177 neuronal activation may not necessarily lead to repeated peptide release, as suggested by the
178 decrease in peptide release over time in **Fig. 2D**. Additionally, fiber photometry cannot provide
179 information about Met- and Leu-Enk independently, as it relies on the precursor gene, *penk*.
180 Taken together, our data highlight the value and importance of coupling fiber photometry results
181 with in vivo measurements of neuropeptides to determine release dynamics.

182 **Predator odor causes the release of Met-Enkephalin in the Nucleus Accumbens Shell**

183 We wanted to test another stressor that is similar in nature to experimenter handling as the
184 experimenter represents aversive visual, olfactory, and touch stimuli to the mouse. Fox odor has
185 been widely demonstrated to be aversive to rodents and other mammalian species [37–39]. The
186 benefit of using predator odor is that it represents what mice would encounter in the wild, outside
187 of the lab environment. It also allows us to probe conserved circuits in laboratory mice related to
188 aversion, threat, and defensive behaviors. Prior reports have shown that predator odor leads to
189 an increase in the expression of the neuronal activation-associated transcription factor fos in
190 enkephalin-positive neurons in different brain regions including the NAcSh [40,41]. Therefore, we
191 sought to determine whether enkephalins are released in the NAcSh following exposure to fox
192 urine. We first measured calcium activity of enkephalinergic neurons using fiber photometry after
193 exposure to fox urine (**Fig. 3A**). We show that upon first exposure, the activity of enkephalinergic
194 neurons is markedly increased (**Fig. 3B-D**). However, this enkephalinergic activity is significantly
195 attenuated during second and third exposures that are separated by five minutes suggesting
196 habituation to the stimulus (**Fig. 3B-D**). To determine whether the response to fox urine may also
197 be due to the novelty of the weigh boat used to introduce the fox urine, we measured

198 enkephalinergic calcium activity after introducing a weigh boat containing water to the home cage
199 (**Suppl. Fig. 4A**). Interestingly, we show that enkephalinergic neurons also respond to the
200 introduction of a novel object, and the response to the water-containing weigh boat is attenuated
201 upon repeated exposure, which is what we observed for fox urine (**Suppl. Fig. 4B-D**). We
202 compared the enkephalinergic neuron activation in response to both water and fox urine for each
203 individual mouse that experienced both, and we see similar calcium transient responses to both
204 the introduction of a novel object and the odor of a predator, suggesting the same subpopulation
205 of enkephalinergic neurons may have been activated (**Suppl Fig. 4E**). Interestingly and
206 importantly, only recently have researchers shown that a higher level of spiking in the striatum is
207 not always reflected in greater photometry transients [42]. In the future, it will be important to
208 determine whether the fox urine response indeed shows higher action potential spiking than the
209 weigh boat with water. Although the calcium responses to both the fox-urine and water-containing
210 weigh boats were similar in magnitude, it may be that different subpopulations of enkephalinergic
211 neurons are activated in the NAcSh. Further exploration of the specific neurons that respond to
212 the introduction of a novel object or the odor of a predator is warranted. We concluded that
213 enkephalinergic neurons are activated by fox odor using fiber photometry. We were then
214 interested in testing whether activation of enkephalinergic neurons leads to release of Met- and
215 Leu-Enk, so we measured peptide levels in the NAcSh after fox odor using our method of
216 microdialysis and nLC-MS (**Fig. 3E**).
217
218 In this separate group of animals, we show that there is a significant increase in Met-Enk release
219 after exposure to fox odor (**Fig. 3F**). The response to predator odor varies appreciably: the
220 responses are almost evenly split between elevated release, release with no elevation, or no
221 detectable release (**Fig. 3G**). Enkephalins are thought to mediate resilience to stress, so the
222 individual differences in responses to predator odor may indicate differences in stress adaptability
223 [32,33,43,44]. Moreover, no sex differences in the responses to fox urine were observed, similar

224 to responses to experimenter handling (**Suppl. Fig. 2B**). It is also worth noting that we only
225 observed Leu-Enk release in 3 of 16 experiments. This is likely due to Leu-Enk not being released
226 following predator odor or because it is released at a level below the LLOQ, as suggested by the
227 observed 3:1 ratio of Met-Enk to Leu-Enk (**Fig. 3G**).
228
229 **Discussion**
230 In summary, this work allows for multiple unique advances in studying endogenous opioids and
231 neuropeptides in general. Although there has been substantial progress in fluorescent sensor-
232 based techniques, electrochemical approaches, and immunoaffinity based assays, the
233 investigation of opioid peptides has lagged due to their unique properties: sequence similarity,
234 diversity, and low concentrations. Here, we address these challenges by advancing microdialysis
235 coupled with nLC-MS. First, we have refined a method of methionine stabilization [21,45,46]that
236 is transferrable to other neuropeptides and have decreased the LLOQ and temporal resolution,
237 which are typically the main critiques of microdialysis and LC-MS approaches. As we have shown,
238 if Met-Enk is not fully oxidized prior to LC-MS analysis, it is hard to quantify because of the
239 presence of differentially oxidized species. The diversity of the signal detected impedes the
240 analysis of a single sample and may lead to inaccurate concentration values. Here, we show that
241 the oxidation of methionine allows for the stable detection of not only Met-Enk but also the
242 simultaneous and selective detection of Leu-Enk.
243
244 Second, we quantified the relationship between Leu- and Met-Enk and offer a definitive *in vivo*
245 ratio (3:1 Met-Enk to Leu-Enk) that has long been in question; this ratio corroborates human data
246 [28] and suggests that mice are a useful model system for the study of enkephalinergic release
247 dynamics. Based on this, future studies investigating the use of opioid peptides as biomarkers for
248 psychiatric conditions will be readily translatable from rodents to humans and will allow for ease
249 in reverse translation efforts. There is already some demonstrated interest in measuring opioid

250 peptide levels in humans due to their roles in mood disorders, substance use, and pain [47,48].
251 Moreover, prior to our study, the predicted ratio of Met- to Leu-Enk was predicted based on the
252 mRNA transcript sequence, so we are the first to confirm that post-translational cleavage indeed
253 yields the predicted ratio. We also noted that Leu-Enk showed a greater fold increase relative to
254 baseline after depolarization with high K+ buffer as compared to Met-Enk. This may be due to
255 increased Leu-Enk packaging in dense core vesicles compared to Met-Enk or since there are two
256 distinct precursor sources for Leu-Enk, namely both proenkephalin and prodynorphin while Met-
257 Enk is mostly cleaved from proenkephalin (see Table 1) [49]. Third, we identify a role for the
258 NAcSh in the acute stress response by demonstrating local release of Met- and Leu-Enk after
259 stress exposure using our improved microdialysis and nLC-MS method. Although studies have
260 suggested a role for the NAcSh in stress through measurements of *penk* transcripts, it had not
261 been definitively shown that there is local release of enkephalins after stress exposure [35,50].
262 Our findings showed a robust increase in peptide release at the beginning of experiments, which
263 we interpreted as due to experimenter handling stress that directly precedes microdialysis
264 collections. However, there are other technical limitations to consider such as the fact that we
265 were collecting samples from mice that were recently operated on. Another consideration is that
266 the circulation of aCSF through the probe may cause a sudden shift in oncotic and hydrostatic
267 forces, leading to increased peptide release to the extracellular space. As such, we wanted to
268 examine our findings using a different technique, so we chose to record calcium activity from
269 enkephalinergic neurons - the same cell population leading to peptide release. Using fiber
270 photometry, we showed that enkephalinergic neurons are activated by stress exposure, both
271 experimenter handling and fox odor, thereby adding more evidence to suggest that
272 enkephalinergic neurons are activated by stress exposure which could explain the heightened
273 peptide levels at the beginning of microdialysis experiments. Repeated experimenter handling led
274 to repeated activation of enkephalinergic neurons. However, fox odor exposure showed
275 significant attenuation after the first exposure. This is consistent with prior studies showing fast

habituation to olfactory stimuli in rodents after initial exposure [37–39,51]. We also showed using fiber photometry that the novelty of the introduction of a foreign object to the cage, before adding fox odor, was sufficient to activate enkephalinergic neurons. This is consistent with the object being a stressor as it is newly introduced to the homecage. Alternatively, it could also mean that the stress response is more nuanced and is impacted by the novelty of the stressor. This is an area of interest to our group, and we will design future experiments to disentangle the novelty from the stressor in order to understand the enkephalinergic system better. Given that previous studies implicating enkephalins in stress used mRNA transcript measurements of proenkephalin, it was not possible to determine whether Leu- and/or Met-Enk were involved in the acute stress response. Our study suggests that both peptides are involved in experimenter handling stress, however this is less clear following exposure to fox odor where Met-Enk appears to be primarily involved. Most of our experiments with fox odor do not show Leu-Enk release, however, that could be due to Leu-Enk levels being below the LLOQ since we have demonstrated that it is 3 times lower than Met-Enk. Fourth, we show that Met- and Leu-Enk are released during acute stress in the NAcSh, offering evidence for their role in gating the stress response, which was suggested based on studies of enkephalins in the Locus Coeruleus [32]. Therefore, combined with other studies, our work suggests that the role of enkephalins in stress is generalizable to other brain regions, namely the ventral striatum. Based on our findings, it remains unclear how enkephalins modulate the stress response. It will be interesting to investigate whether enkephalinergic signaling modulates stress coping behaviors. Future studies will focus on determining the effect of the local release of Met- and Leu-Enk in the NAcSh on responses to stress in rodents.

Finally, when a limited amount of peptide is released over time, we show that peptide release is biologically constrained and can be experimentally driven using high K+ buffer or photo or chemogenetic stimulation [13]. We also show that data from fiber photometry corroborate peptide release data; however, fiber photometry does not offer the necessary specificity to correlate

activation with release, or the distinction between different peptides that arise from the same precursor molecule. Additionally, it is important to stress that our fiber photometry studies used a calcium sensor as a proxy for neuronal activity and the temporal scale was on the order of seconds. A recent study using an opioid-peptide fluorescent sensor shows temporal scales on the order of minutes, which mirrors microdialysis timelines for neuropeptide detection, and offers evidence that neuropeptide dynamics are generally much slower than neurotransmitters *in vivo* [52]. In conclusion, this improved peptide detection method enables biological advances through an optimized approach for Met- and Leu-Enk detection *in vivo* with broad applicability to other neuropeptides.

Figures and Legends:

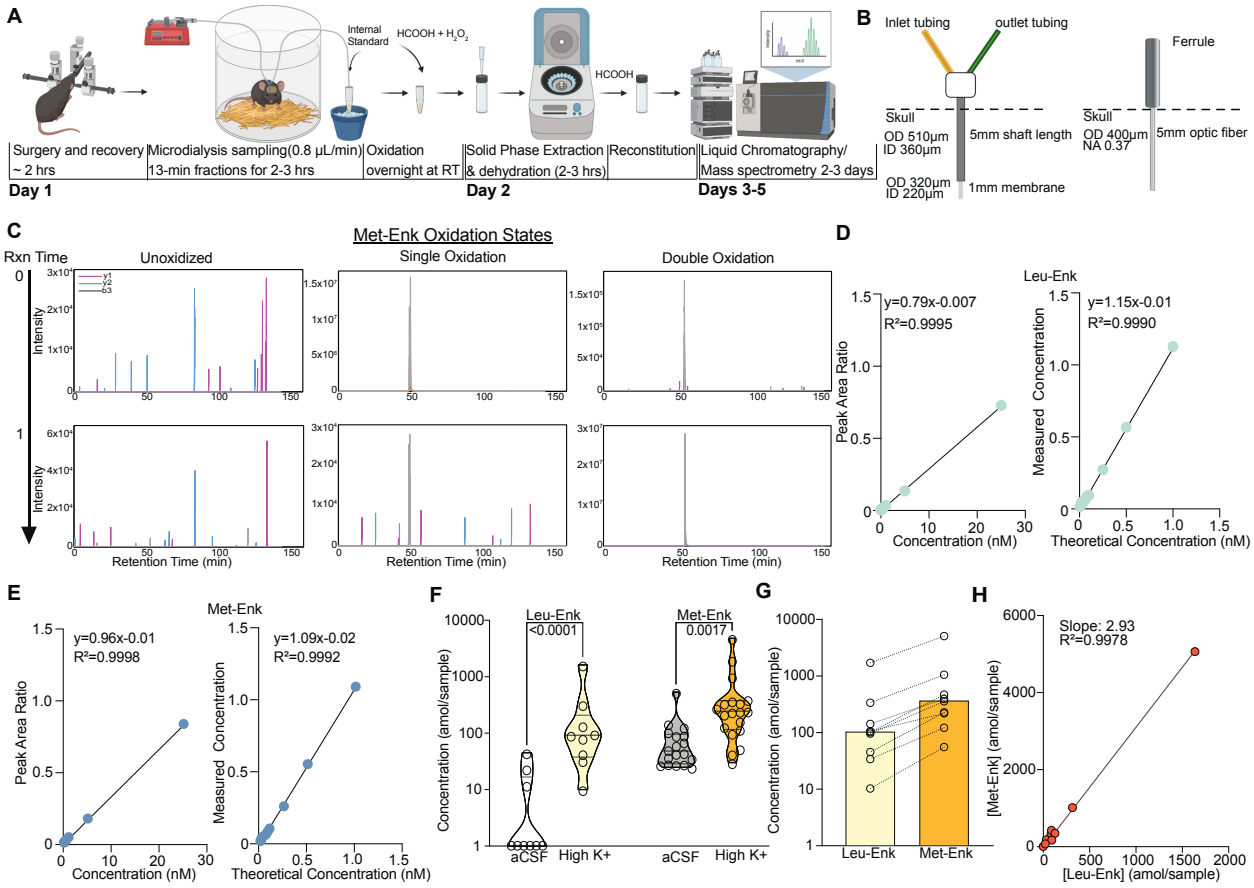

Figure 1: An optimized approach for *in vivo* Met- and Leu-Enk measurement. **A.** Timeline of *in vivo* sample collection on day 1 and methionine oxidation reaction overnight, sample processing on day 2, and data acquisition on the LC-MS, days 3-5. The microdialysis probe is implanted via stereotaxic surgery in the Nucleus Accumbens Shell. The mouse is allowed to recover before being connected to the microdialysis lines. Samples are then collected at a rate of 0.8 μL/min for 13 minutes each. After collection is completed, the samples are oxidized overnight. On day 2 the samples undergo solid phase extraction (SPE) and are then dehydrated and reconstituted using formic acid (HCOOH) before being acquired on the LC-MS. **B**. Custom microdialysis probe specifications including membrane size and inner and outer diameters (ID and OD respectively) compared to fiber photometry probe specifications including OD of optic fiber and numerical aperture (NA). **C**. Before the methionine oxidation at reaction (Rxn) time 0, Met-Enk exists in three different forms with varying intensities, unoxidized (multi-peak), singly oxidized (multi-peak), and doubly oxidized (single peak). After the reaction completes (Rxn time 1), most of the detected signal is in the doubly oxidized form and shows a single peak (>99% signal intensity). Y1, y2, b3 refer to the different elution fragments resulting from Met-Enk during LC-MS. **D.** (Left) Forward calibration curve of Leu-Enk and Met-Enk showing the peak area ratios as the light standard levels are varied. **(**Right**)** Reverse calibration curve of Leu-Enk showing the relationship between the heavy standard concentration applied and the measured concentration based on the instrument. **E.** Same setup as **D** but for Met-Enk**. F.** Violin plots showing that high K+ ringer's solution increases the release of both Leu-Enk and Met-Enk compared to baseline levels in artificial cerebrospinal fluid (aCSF) (Leu-Enk n=9, Met-Enk n=18). The dashed center line indicates the median. **G.** The evoked concentrations of Met-Enk to Leu-Enk in the same samples show that Met-Enk is consistently released at a higher level than Leu-Enk (n=9). **H.** Met-Enk is released at a factor of 2.97 that of Leu-Enk as shown by linear regression analysis of the data in f, suggesting a linear relationship between the two peptides. Data in **F**, **G**, and **H** are transformed to a log scale. In **F**, 2-way ANOVA analysis shows a main effect of peptide ($F(1, 51) = 32.30$, $p<.0001$), solution ($F(1, 51) = 50.04$, $p<.0001$), and interaction ($F(1, 51) = 9.119$, $p=.0039$). The *p*-values reported were calculated using a Sidak's multiple comparisons test. Mean difference between baseline Leu-Enk and high K+ 1.533, Mean difference between baseline Met-Enk and high K+ 0.6157 , 95% confidence interval 0.3074 to 1.527 ($\log_{10}$ values).

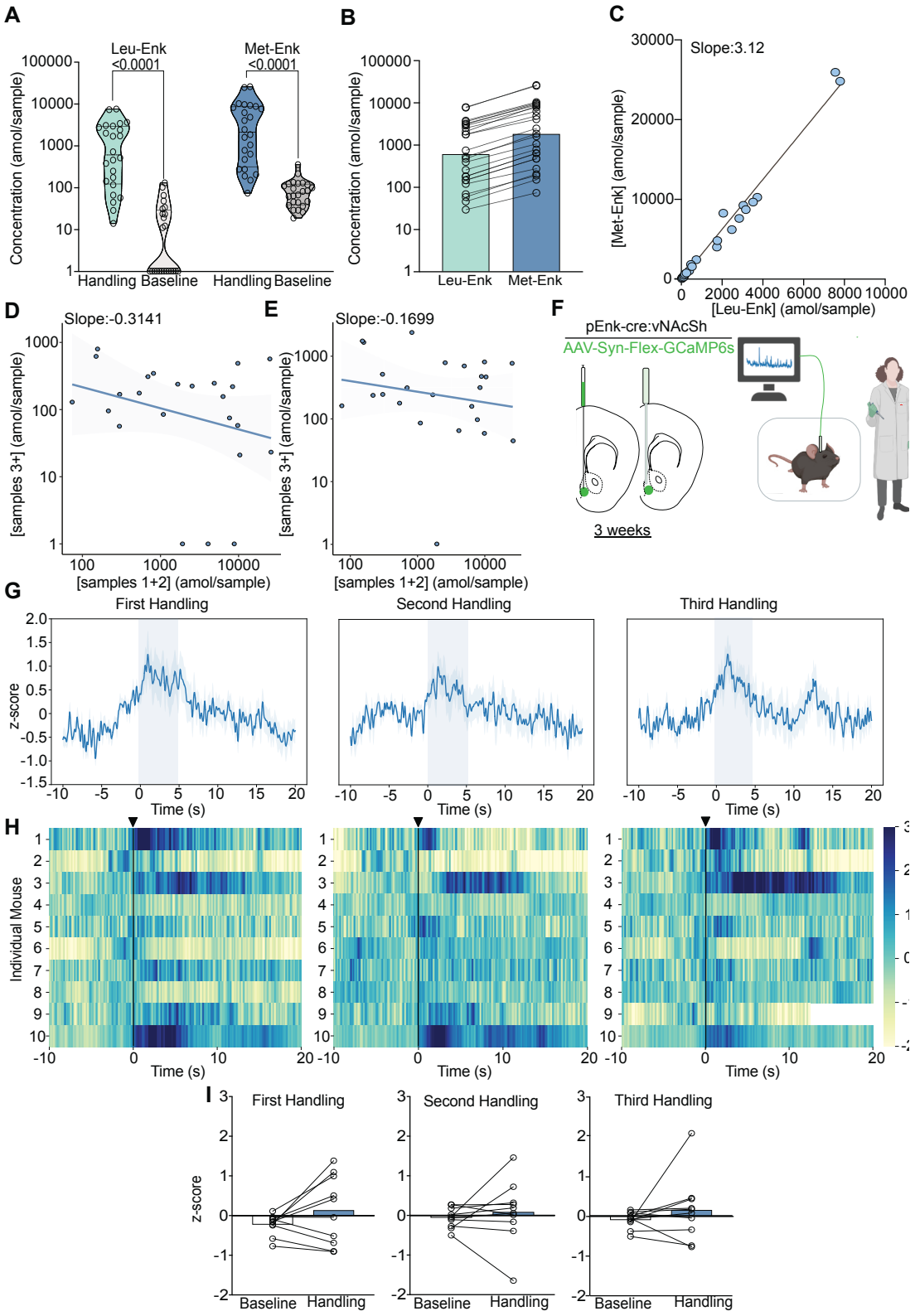

346
347
348
349
350

Figure 2: Experimenter handling evokes the release of Met- and Leu-Enk in the NAcSh. A. Experimenter handling during microdialysis causes a significant increase in the release of Leu- and Met-Enk in comparison to baseline. 2-way ANOVA on log-transformed data showing a significant effect of peptide $F(1,92)=32.58$, $p<0.0001$, handling $F(1,92)=146.1$, $p<.0001$, and interaction $F(1,92)=4.778$, $p=.0314$, Sidak's multiple comparisons test was conducted and *p*-values are shown on the figure. Mean difference between baseline Leu-Enk and handling 2.055, Mean difference between baseline Met-Enk and handling 1.426, 95% confidence interval 0.05751 to 1.201 ($\log_{10}$ values).**B.** During experimenter handling, Met-Enk is consistently released at a higher rate than Leu-Enk in the same samples. **C.** Linear regression analysis of the data in **B** shows that Met-enk is released at a rate of 3.12 times the rate of Leu-Enk during experimenter handling suggesting a linear relationship between the two peptides. **D.** A negative correlation (-0.3141) shows that if a high concentration of Met-Enk is released in the first two samples, the concentration released in later samples is affected; such influence suggests that there is regulation of the maximum amount of peptide to be released in NAcSh. **E.** The negative correlation in panel d is reversed by using high K+ buffer with a negative correlation coefficient of -0.1699 to evoke Met-Enk release, suggesting that the limited release observed in **D** is due to modulation of peptide release rather than depletion of reserves. Data in **A-E** are transformed to a log scale and n=24 animals. In panel **A**, 2-way ANOVA analysis shows a main effect of peptide, treatment, and interaction. The *p*-values reported were calculated using a Sidak's multiple comparisons test. **F.** Schematic describing the viral strategy and probe placement for the fiber photometry experiment in pEnk-Cre mice injected with the calcium sensor GCaMP6s in the NAcSh. **G.** Average z-score trace following the first, second, and third events involving experimenter handling. **H**. Heatmaps showing individual mouse z-scored fiber photometry responses before and after experimenter handling. **I**. Bar graphs showing the averaged z-score responses before experimenter handling and after experimenter handling (n=10 for **G-I**).

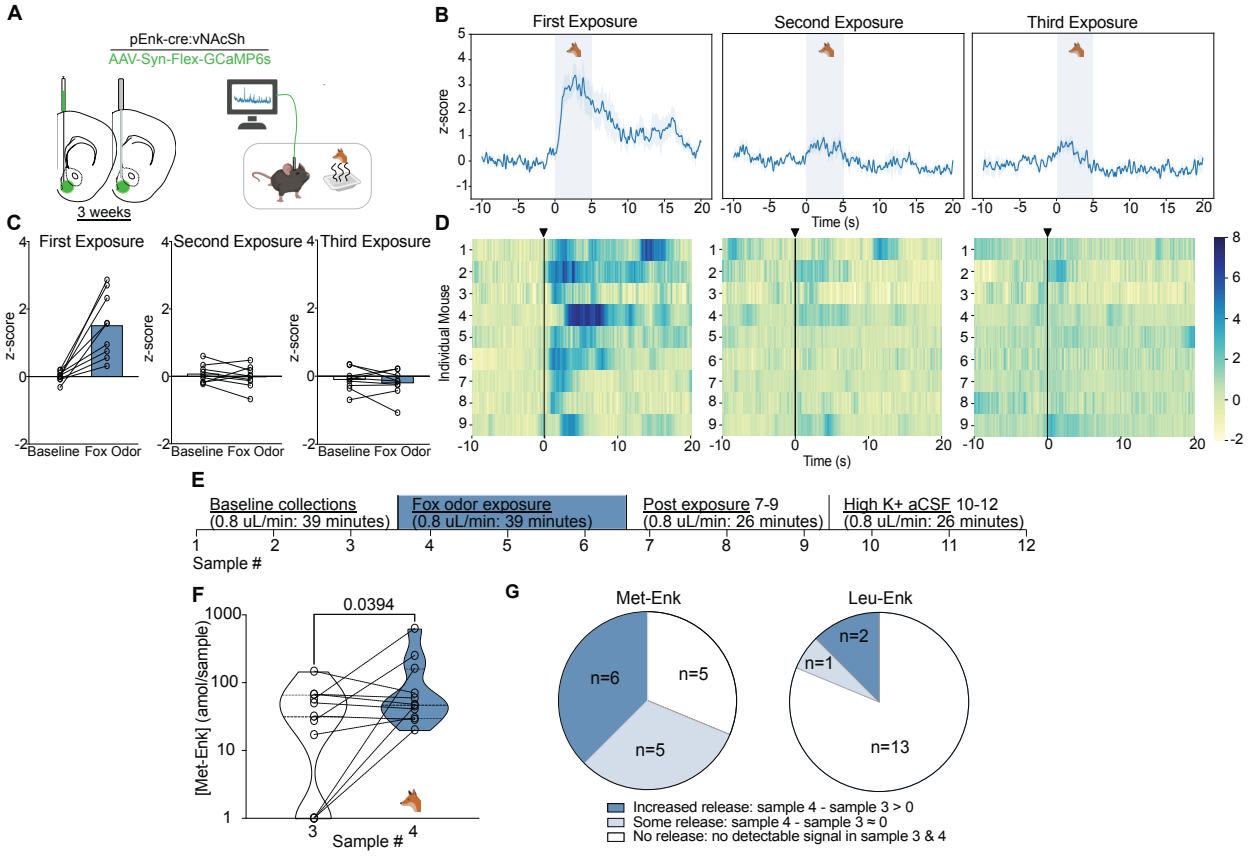
A
pEnk-cre:vNAcSh
AAV-Syn-Flex-GCaMP6s
3 weeks
B
First Exposure
Second Exposure
Third Exposure
z-score
Time (s)
C
First Exposure
Second Exposure
Third Exposure
z-score
Baseline Fox Odor
D
Individual Mouse
Time (s)
E
Baseline collections
(0.8 uL/min: 39 minutes)
Fox odor exposure
(0.8 uL/min: 39 minutes)
Post exposure 7-9
(0.8 uL/min: 26 minutes)
High K+ aCSF 10-12
(0.8 uL/min: 26 minutes)
Sample #
F
0.0394
[Met-Enk] (amol/sample)
Sample #
G
Met-Enk
Leu-Enk
n=6
n=5
n=5
n=2
n=1
n=13
Increased release: sample 4 - sample 3 > 0
Some release: sample 4 - sample 3 ≈ 0
No release: no detectable signal in sample 3 & 4

377
378

Figure 3. Fox odor exposure activates enkephalinergic neurons and drives the release of Met-Enk in the NAcSh. A. Viral strategy and probe placement for the fiber photometry experiment in pEnk-Cre mice injected with the calcium sensor GCaMP6s in the NAcSh. **B.** Averaged z-score traces of the first, second, and third exposure to fox odor. **C.** Bar graphs showing the averaged z-scored fiber photometry responses before and after exposure to fox odor **D**. Heatmaps showing individual mouse z-scored fiber photometry responses before and after exposure to fox odor. (n=9, for **A-D**) **E**. Experimental timeline describing the fox odor microdialysis experiment. **F**. There is a significant increase in Met-Enk concentration during fox odor exposure (sample 4), in comparison to sample, 3 before odor exposure. Data is transformed to a log scale and the *p*-value was calculated using a two-tailed paired t-test (n=11), t=2.369, df=10, mean difference 0.1388, 95% confidence interval -0.5419 to 0.2644 **G.** Pie charts showing the variation across animals in Met-Enk and Leu-Enk release profiles in response to exposure to fox odor, suggesting that such exposure may selectively cause the release of Met-Enk but not Leu-Enk. Increased release showed higher concentration of Met-Enk during exposure to fox odor (sample 4) than the sample before (sample 3), some release showed a comparable level to the sample before exposure, and no release showed no quantifiable concentration during exposure to fox odor.

397 **Materials and Methods:**

398 **List of Abbreviatons:**

399 FA, formic acid
400 MeCN, acetonitrile
401 MeOH, methanol
402 DIA, Data-Independent Acquisition
403 AGC, Automatic Gain Control
404 *nano*-LC-MS, capillary liquid chromatography interfaced to a mass spectrometer
405 MS1, mass spectra of peptide precursors
406 MS2, fragmentation mass spectrum of peptide from precursor ion
407
408 **Reagents**

409 Acetonitrile (MeCN; J.T. Baker, cat. no. 9829-03)

410 Water (J.T. Baker, cat. no. 4218-03)

411 Formic Acid (FA; Sigma-Aldrich, cat. no. 56302)

412 Hydrogen Peroxide (Fisher Chemical, cat. no. H325-100)

413 Methanol (MeOH; Fluka, cat. no. 34966)

414 **Equipment**

415 Stage tips

416 Laboratory pipetting needles with 90° blunt ends, 16-gauge, 2-inch length; Cadence Science,
417 cat. no. 7938)

418 C18 extraction disks, diam. = 47 mm, 20 pack; (Empore, cat. no. 66883-U)

419 Adapter for stage tipping (Glygen, cat. no. CEN.24)

420 1.5-ml tubes (Axygen, Cat. No. MCT-175-C)
421 Eppendorf centrifuge (Eppendorf, model 5424R)

422 Vortex (Labnet VX100)

423 Autosampler vials (Sun-Sri, Cat. No. 200046)

424 Autosampler vial caps (Sun-Sri, cat. no. 501 382)

425 UPLC system for LC-MS of analysis of TMT-labeled peptides (EASY nL-LC 1000, Thermo
426 Scientific)

427 Mass spectrometer for analysis of TMT-labeled peptides (Q-Exactive™ Plus Hybrid Quadrupole
428 Orbitrap™, Thermo Scientific)

429 EASY-Spray™ column, 75 µm x 50 cm PepMap (Thermo Scientific™, cat. no. ES903)

430

431

432 **Animals**

433 Adult male and female C57BL/6 mice at 8-15 weeks of age were used for microdialysis
434 procedures. For fiber photometry, adult preproEnkephalin-Cre (pEnk-Cre) [53] male and female
435 mice at ages between 15-24 weeks of age were used to measure enkephalinergic cell activity.
436 Mice were group housed and kept at a 12-hour light/dark cycle with *ad libitum* access to water
437 and food. The holding facility was both temperature and humidity controlled. All surgical and
438 behavioral procedures were approved by the Washington University School of Medicine animal
439 care guidelines in accordance with federal animal use regulations.

440 **Chemicals**

441 Met and Leu Enkephalin standards including isotopically labeled forms were synthesized at New
442 England Peptide and can be ordered by the research community. The heavy isotope labeled Leu
443 Enkephalin is synthesized with a fully labeled L-Leucine ($^{13}C_6$, ^{15}N) at the C terminus of the peptide
444 (YGGF**L**). For Met Enkephalin, a fully labeled L-Phenylalanine ($^{13}C_9$, ^{15}N) was added (YGG**F**M).
445 The resulting mass shift between the endogenous (light) and heavy isotope-labeled peptide are
446 7Da and 10Da, respectively. Heavy isotope amino acids are guaranteed >99% pure. Peptide
447 purity specifications are set at ≥ 95% pure by area on a regular HPLC gradient with UV detection.
448 Artificial cerebrospinal fluid (aCSF) contained 124 mM NaCl, 2.5 mM KCl, 2 mM $CaCl_2$, 1 mM
449 $MgCl_2$, 1.25 mM NaH_2PO_4, 24 mM $NaHCO_3$, 5 mM HEPES, 12.5 mM Glucose adjusted to pH 7.4
450 with NaOH. High K^+ ringer solution contained 48 mM NaCl, 100 mM KCl, 2.4 mM $CaCl_2$, 0.85 mM
451 $MgCl_2$ adjusted to pH 7.4 with NaOH as described in (Al-Hasani, 2018). All salt compounds were
452 purchased from Sigma (St. Louis, MO).

453 ***In vivo* microdialysis**

454 Custom microdialysis probes (BASI Inc. part MD-2206) of 5 mm shaft length and 1 mm
455 Polyacrylonitrile membrane with a 30 kDa molecular weight cutoff were used for the *in vivo*
456 experiments. The probes were flushed prior to surgical implantation for 15 minutes at 10 μL/min
457 with artificial cerebrospinal fluid as directed by the manufacturer using a BASI syringe pump (MD

458 1001). For the surgical procedure, mice were briefly anaesthetized in an induction chamber at 3%
459 isofluorane before being placed in a stereotaxic frame (Kopf) secured with ear and bite bars.
460 During the surgery, the isofluorane level was kept at 1.5-2%. The probe was then inserted into
461 the ventral Nucleus Accumbens shell (stereotaxic coordinates from bregma: +1.3 [AP], ±0.5 [ML],
462 −5.0 mm [DV]). Implanted probes were secured with dental adhesive (C&B metabond kit) followed
463 by cyanoacrylate (Loctite superglue gel control).
464 After the completion of the surgery, each mouse was allowed to recover for 30 minutes. The
465 mouse was then connected to an inlet perfusion line to circulate aCSF or high K+ ringer solution
466 and an outlet perfusion line to collect the interstitial fluid from the NAcSh. The outlet line directly
467 collected sample in a tube that is kept at 4 °C throughout the experiment. The flow of aCSF was
468 then then turned on and sample collection time started as sample began to collect in the outlet
469 tube. The flow rate of aCSF was set to 0.8 μL/min during sample collection. Fractions were
470 collected every 13 minutes resulting in a 10 μL sample. After each collection, the samples were
471 spiked with 2 μL of 12.5 fmol isotopically labeled Met-Enkephalin and Leu-Enkephalin. The
472 microdialysis rig (BASI Raturn MD 1404) was equipped with bedding, regular mouse chow and
473 water ad libitum. While connected to the perfusion lines, the mice were allowed to move freely.
474 For the experiments measuring evoked release, the high K+ ringer solution was perfused through
475 the lines instead of aCSF at 0.8 μL/min and fractions were collected every 13 minutes as
476 described previously. The samples were similarly spiked with 2 μL of 12.5 fmol isotopically labeled
477 Met-Enkephalin and Leu-Enkephalin.
478 For the experiments where the animals were exposed to the fox urine odor, 3 mL of fox urine was
479 absorbed into a kim wipe contained in a chemical weigh boat. The weigh boats were prepared
480 and remained in a fume hood the experiment to prevent the odor permeating the experimental
481 space before the planned collection. Then, the experimenter placed the weigh boat in the
482 microdialysis rig and allowed the mouse to explore it. The exposure was standardized to span 3

483 fractions (39 minutes) during each of the experiments while aCSF was being perfused through
484 the lines.

485 **In vivo sample processing**

486 ***Methionine Oxidation Reaction***

487 For met-enkephalin detection and stabilization, the animal samples underwent a methionine
488 oxidation reaction [21]. To each sample vial, 28 μl of 0.1% (vol/vol) formic acid (FA) was added
489 and then the samples were transferred to 0.5 mL tubes from the collection tubes. Afterwards, 40
490 μl of a mixture of 6% FA (vol/vol) and 6% hydrogen peroxide (vol/vol) was added to each of the
491 sample tubes and mixed and gently spun. The samples were then incubated overnight at room
492 temperature.

493 ***Solid Phase Extraction with C18 stage tips***

494 After the methionine oxidation reaction, a solid phase extraction process was performed using
495 C18 stage tips. Stage tips were conditioned before sample loading. To each of the stage tips, 100
496 μl of methanol is added and then spun for 2 minutes at 2,000 rpm in microcentrifuge tubes. The
497 stage tips were then rinsed with 100 μl of a mixture of 50% acetonitrile (MeCN; (vol/vol)) and 0.1%
498 FA (vol/vol) followed by a 2-minute spin at 2,000 rpm. This was followed by a rinse in 0.1% FA
499 (vol/vol) and a 2-minute spin at 3,000 rpm. The final rinse was done by adding 100 μl of 1% FA
500 (vol/vol) to each of the stage tips. Following the final rinse, the samples were added to the C18
501 stage tips and spun for 10 minutes at 0.8 rpm. After ensuring that the samples passed through
502 the stage tips, the samples were desalted with 0.1% FA (vol/vol) and spun for 1.5 minutes at
503 3,000 rpm twice. After the spins were done, the stage tips were directly placed into autosampler
504 vials to elute the analyte with 60 μl of 50% MeCN, 0.1% FA (vol/vol) using a syringe. Eluates in
505 the autosampler vial were dried in a speedvac, reconstituted in 3 μl 1% FA (vol/vol) and set up on
506 the autosampler for injection on the mass spectrometer.

507 ***Nano*-LC-MS/MS.** The samples in formic acid (1%) were loaded (2.5 µl) onto a 75 µm i.d. × 50
508 cm Acclaim® PepMap 100 C18 RSLC column (Thermo-Fisher Scientific) on an EASY *nano*LC
509 (Thermo Fisher Scientific) at a constant pressure of 700 bar at 100% A (1%FA). Prior to sample
510 loading the column was equilibrated to 100%A for a total of 11 µL at 700 bar pressure. Peptide
511 chromatography was initiated with mobile phase A (1% FA) containing 5%B (100%MeCN, 1%FA)
512 for 1 min, then increased to 20% B over 19 min, to 32% B over 10 min, to 95% B over 1 min and
513 held at 95% B for 19 min, with a flow rate of 250 nL/min. The data was acquired in data-
514 independent acquisition (DIA) mode. The full-scan mass spectra were acquired with the Orbitrap
515 mass analyzer with a scan range of *m/z* = 150 to 1500 and a mass resolving power set to 70,000.
516 Data-independent (DIA) high-energy collisional dissociations were performed according to the
517 inclusion list with a mass resolving power set to 17,500, an isolation width of 2 Da, and a
518 normalized collision energy setting of 27. The maximum injection time was 60 ms for parent-ion
519 analysis and product-ion analysis. The automatic gain control (AGC) was set at a target value of
520 3e6 ions for full MS scans and 2e5 ions for MS2. The inclusion list contained 4 peptide entries.
521 The loop count was set at 30. Retention time windows were set at 20 min. Each sample was run
522 in two technical replicates and the peak area ratio was averaged before concentration calculations
523 of the peptides were conducted. Several quality control steps were conducted prior to running the
524 *in vivo* samples. 1) Two technical replicates of a known concentration were injected and analyzed
525 – an example table from 4 random experiments included in this manuscript is shown below. 2)
526 The buffers used on the day of the experiment (aCSF and high K+ buffer) were also tested for
527 any contaminating Met-Enk or Leu-Enk signals by injecting two technical replicates for each
528 buffer. Once these two criteria were met, the experiment was analyzed through the system. If
529 either step failed, which happened a few times, the samples were frozen and the machines were
530 cleaned and restarted until the quality control measures were met.

Injected conc (aM)	QC before ME (aM)	QC after ME (aM)	Mean	STDEV	QC before LE (aM)	QC after LE (aM)	Mean	STDEV
25 fM	28	32	30.000	2.82842712	40	36	38	2.82842712

40 aM	44	41	42.500	2.12132034	53	50	51.5	2.12132034
40 aM	54	51	52.500	2.12132034	51	55	53	2.82842712
40 aM	42	41	41.500	0.70710678	43	45	44	1.41421356

Stable-isotope dilution assay for measurement of enkephalins

Peptides were synthesized as high purity natural abundance and stable isotope-labeled pairs for the development of a targeted proteomics method for enkephalins. Assays were developed as Tier 2 assays according to CPTAC guidelines [22]. Co-eluting peak boundaries for the internal standard and endogenous peptides were manually refined using the Skyline software package [54]. Integrated peak areas for the three most intense fragment ions were then exported for determination of peak area ratios of endogenous to internal standard signal, which were used as a basis for determining abundance and quantifying changes in enkephalin levels in mouse studies.

***In vivo* fiber photometry**

Stereotaxic surgery

For the surgical procedure, pEnk-Cre mice were briefly anaesthetized in an induction chamber at 3% isofluorane before being placed in a stereotaxic frame (Kopf) secured with ear and bite bars. During the surgery, the isofluorane level was kept at 1.5-2%. Then we performed a craniotomy and unilaterally injected using a Nanoject III (Drummond) 200-250 nL of AAV5.Syn.Flex.GCaMP6s.WPRE.SV40 (Addgene: 100845-AAV5) at the following coordinates :+1.3 [AP],±0.5 [ML], −5.0 mm [DV]. To allow for viral expression, the fiber photometry probes (5 mm shaft length, doric lenses) were implanted 3 weeks later at +1.3 [AP], ±0.5 [ML], −4.75 mm [DV]. Implanted probes were secured with dental adhesive (C&B metabond kit) followed by cyanoacrylate (Loctite superglue gel control).

Fiber photometry recording procedure

Before recording, the implanted probes were tethered to an optic fiber using a ferrule sleeve (Doric, catalog no. ZR_2.5). Two light-emitting diodes (LEDs) were used to excite GCaMP6s. A

556 331 Hz sinusoidal LED light (Doric) of wavelength 470 nm 470 ± 20 nm was used for the Ca^{2+} -
557 dependent signal. A 210 Hz sinusoidal LED light of wavelength 405 ± 10 nm (Doric, LED driver)
558 was used to evoke the Ca^{2+} -independent signal and serve as the isosbestic control. GCaMP6s
559 fluorescence traveled through the same optic fiber before being bandpass filtered (525 ± 25 nm,
560 Doric, catalog no. FMC4), transduced by a femtowatt photoreceiver (New Focus Model 2151) and
561 recorded by a real-time processor (TDT, RZ5P). The signals were extracted by the Synapse
562 software (TDT). During the recording, two behavioral manipulations were introduced. The first
563 was after a 10-minute recording in a home cage environment, an experimenter handled the
564 mouse while the recording was ongoing. The handling bout which mimicked traditional scruffing
565 lasted about 3-5 seconds. The mouse was then let go and the handling was repeated another
566 two times in a single session with a minimum of 1-2 minutes between handling bouts. Mice were
567 habituated to this manipulation by being attached to the fiber photometry rig, for 3-5 consecutive
568 days prior to the experimental recording. Additionally, the same maneuver was employed when
569 attaching/detaching the fiber photometry cord, so the mice were subjected to the same process
570 several times. The second behavioral manipulation was introduced to the same mice a week after
571 the first recording session. After a 10-minute recording in the home-cage environment, a
572 weighboat containing a kim wipe that had absorbed 3 mL of fox urine was placed in the cage as
573 the recording proceeded. The weigh boat was removed after a minute of exploration then re-
574 introduced into the cage for another two times, separated by 5 minutes from the last exposure,
575 during the session. In a subset of the animals (5 of 9), the fox urine exposure was preceded by
576 water exposure following the same process described above in the same recording session.

577 Fiber Photometry Data Analysis

578 Data analysis was performed through the python toolbox GuPPy [55]. Briefly, the isosbestic
579 control signal was used to correct for motion and photobleaching artifacts. The control channel is
580 fitted to the signal channel using a least squares polynomial fit of degree 1. Transient detection
581 occurred after using a 15s moving window for thresholding transients. Then, high-amplitude

582 events were identified and their timestamp of occurrence during the session was reported. To
583 determine the effect of handling or fox urine exposure on enkephalinergic cell activity, the event
584 timestamp was used to observe changes in activity before and after the behavioral manipulation.
585 The average of all trials is then calculated for repeated exposures and for exposures in multiple
586 animals. The fiber photometry data was represented as z-scores.

587 Immunohistochemistry and verification of probe placement

588 After the completion of the experiment, mice were anaesthetized with a mixture of ketamine,
589 xylazine and acepromazine and transcardially perfused with ice-cold 4% paraformaldehyde in
590 phosphate buffer. After the perfusion, brains were dissected and fixed for 24 hours in 4%
591 paraformaldehyde at 4°C and then placed in 30% sucrose solution for cryoprotection for a
592 minimum of 48 hours. The brains were then sliced into 30 um sections, washed three times in
593 PBS and blocked in PBS containing 0.5% Triton X-100 and 5% goat serum for one hour. Following
594 the blocking step, the slices were stained for the glial fibrillary acidic protein (GFAP), an astrocyte
595 marker to determine glial scarring around the probe site (guinea pig anti-GFAP, synaptic systems)
596 at 1:500 dilution and incubated at 4°C for 16 hours. The next day, the sections were washed three
597 times with PBS and stained with the secondary antibody, mouse anti-guinea pig, Alexa Fluor 594
598 (Invitrogen) at 1:500 dilution and incubated for two hours at room temperature. After the
599 incubation, the slices were washed three times in PBS, followed by two washes with PB. Finally,
600 the slices were mounted on glass slides with Hard set Vectashield with DAPI staining (Vector
601 Labs) and imaged using an epifluorescence microscope (Leica DM6 B). Correct probe placement
602 in the NAcSh is represented in **supplementary figure 1B**.
603 For the verification of the injection and probe placement for fiber photometry, the same procedure
604 described above was performed for tissue preparation. After slicing, the slices were washed in a
605 0.1% Triton for one hour in order to permeabilize the cells followed by two 10-minute PBS washes.
606 The slices were then stained with Neurotrace (Nissl) red (Invitrogen) to mark neurons by adding
607 5 μL to each well for 2 hours at room temperature followed by 3 10-minute PBS washes and 3

608 10-minute PB washes. Finally, the slices were mounted using Hard set Vectashield (Vector Labs).
609 GCaMP6s expression was determined by observing green fluorescent protein expression
610 colocalized with Neurotrace staining. Correct probe placement in the NAcSh is represented in
611 **supplementary figure 1D**.

612 **Statistical Analysis**

613 We performed simple linear regression analysis on the forward and reverse curves and reported
614 the line equations. For the forward curves, the regression was applied to the measured
615 concentration of the light standard as the theoretical concentration was increased. For plotting
616 purposes, we show the measured peak area ratios for the light standards in the forward curves.
617 For the reverse curves, the regression was applied to the measured concentration of the heavy
618 standard, as the theoretical concentration was varied. The proteomics data is represented as
619 violin plots with individual points depicted and dashed lines indicating quartiles. The middle-
620 dashed lines represent the median. The violin plots were created using Graphpad Prism. The
621 data was $\log_{10}$ transformed to reduce the skewness of the dataset caused by the variable range
622 of concentrations measured across experiments/animals. Prior to log transformation, the
623 measurements failed normality testing for a Gaussian distribution. After the log transformation,
624 the data passed normality testing, which provided the rationale for the use of statistical analyses
625 that assume normality. Two-way ANOVA testing with peptide (Met-Enk or Leu-Enk) and
626 treatment (buffer or stress for example) as the two independent variables. Post-hoc testing was
627 done using Šídák's multiple comparisons test and the *p* values for each of these analyses are
628 shown in the figures (Figs. 1F, 2A). A paired t-test was performed on the predator odor proteomic
629 data before and after odor exposure to test that hypothesis that Met-Enk increases following
630 exposure to predator odor (Fig. 3F). These analyses were conducted using Graphpad Prism. To
631 determine the linear relationship between the levels of Met-Enk to Leu-Enk in the same samples,
632 we conducted simple linear regression analysis and reported the slopes of the lines. This is based
633 on prior literature positing a relatively fixed ratio of Met-Enk to Leu-Enk, and we corroborate that

634 here [25–27]. For the fiber photometry data, the z-scores were calculated as described in using
635 GuPPy which is an open-source python toolbox for fiber photometry analysis [55]. The z-score
636 equation used in GuPPy is z=(ΔF/F-(mean of ΔF/F)/standard deviation of ΔF/F) where F refers to
637 fluorescence of the GCaMP6s signal. For the averaged plots depicted in Fig. 2 and Fig. 3, z-
638 scores from all individual animals were averaged and shown as one trace with the SEM as the
639 highlighted area. The purpose of the averaged traces is to show the extent of concordance of the
640 response to experimenter handling and predator odor stress among animals with the SEM
641 demonstrating that variability. The heatmaps depict the individual responses of each animal. The
642 heatmaps were plotted using Seaborn in Python and mean traces were plotted using Matplotlib
643 in Python.
644

645 **Funding**
646 This work was supported by National Institutes on Drug Abuse R00 DA038725 (RA) and
647 R21DA048650 (RA). The NARSAD Young Investigator Grant from the Brain and Behavior
648 Research Foundation, grant no. 28243 (RA). The WU-PSR is supported in part by the WU Institute
649 of Clinical and Translational Sciences (NCATS UL1 TR000448), the Mass Spectrometry
650 Research Resource (NIGMS P41 GM103422; R24GM136766) and the Siteman Comprehensive
651 Cancer Center Support Grant (NCI P30 CA091842). Cognitive, Computational, and Systems
652 Neuroscience Fellowship (MOM).

653 **Author Contributions**

654 - Conceptualization: RA, MOM, RRT, RS
655 - Methodology: MOM, RA, PEG, RC, JM, RS
656 - Investigation: MOM, PEG, RC, SMC, JW
657 - Formal Analysis: MOM, PEG, RS
658 - Visualization: MOM, JM

- Supervision: RA, RRT, RS
- Writing—original draft: MOM, PEG, RS
- Writing—review & editing: RA, MOM, PEG, RC, SMC, JM, JW, RS, RRT

Acknowledgments

The figure schematics were created with biorender.com. We would like to thank the Moron-Concepcion lab for providing us with the Enk-Cre mouse line. We would like to thank Justin W. Baldwin for his guidance on appropriate data visualization tools and for his support in proofreading the manuscript. We would also like to thank Dr. Jordan McCall for his advice on data analysis and visualization as well as proofreading the manuscript. Thank you to Emily Wheeler for proofreading the manuscript and providing feedback on sentence structure and flow. We would also like to thank the entirety of the proteomics core team including Dr. Yiling Mi for her assistance. Thank you to the entirety of the Al-Hasani and McCall labs for their feedback on experimental design and analysis. Finally, thank you to Dr. Tim Holy, Dr. Robyn Klein, and Dr. Alexxai Kravitz for their feedback.

References

[1] L.D. Fricker, E.B. Margolis, I. Gomes, L.A. Devi, Five Decades of Research on Opioid Peptides: Current Knowledge and Unanswered Questions, Mol Pharmacol 98 (2020) 96–108. https://doi.org/10.1124/MOL.120.119388.

[2] M.R. Banghart, X.J. He, B.L. Sabatini, A Caged Enkephalin Optimized for Simultaneously Probing Mu and Delta Opioid Receptors, ACS Chem Neurosci 9 (2018) 684–690. https://doi.org/10.1021/ACSCHEMNEURO.7B00485/ASSET/IMAGES/LARGE/CN-2017-00485A_0003.JPEG.

[3] I. Gomes, S. Sierra, L. Lueptow, A. Gupta, S. Gouty, E.B. Margolis, B.M. Cox, L.A. Devi, Biased signaling by endogenous opioid peptides, Proceedings of the National Academy of Sciences 117 (2020) 11820–11828. https://doi.org/10.1073/pnas.2000712117.

[4] A. Mansour, M.T. Hoversten, L.P. Taylor, S.J. Watson, H. Akil, The cloned μ, δ and κ receptors and their endogenous ligands: Evidence for two opioid peptide recognition cores, Brain Res 700 (1995) 89–98. https://doi.org/10.1016/0006-8993(95)00928-J.

[5] M.R. Banghart, S.Q. Neufeld, N.C. Wong, B.L. Sabatini, Enkephalin Disinhibits Mu Opioid Receptor-Rich Striatal Patches via Delta Opioid Receptors, Neuron 88 (2015) 1227–1239. https://doi.org/10.1016/J.NEURON.2015.11.010.

[6] N.T. Maidment, D.R. Brumbaugh, V.D. Rudolph, E. Erdelyi, C.J. Evans, Microdialysis of extracellular endogenous opioid peptides from rat brain in vivo, Neuroscience 33 (1989) 549–557. https://doi.org/10.1016/0306-4522(89)90407-7.

[7] P.W. Marinelli, L. Bai, R. Quirion, C. Gianoulakis, A Microdialysis Profile of Met-Enkephalin Release in the Rat Nucleus Accumbens Following Alcohol Administration, Alcohol Clin Exp Res 29 (2005) 1821–1828. https://doi.org/10.1097/01.alc.0000183008.62955.2e.

[8] L. Hemandez, B.G. Hoebel, Food reward and cocaine increase extracellular dopamine in the nucleus accumbens as measured by microdialysis, 1988.

[9] M.M. Nieto, J. Wilson, A. Cupo, B.P. Roques, F. Noble, Chronic Morphine Treatment Modulates the Extracellular Levels of Endogenous Enkephalins in Rat Brain Structures Involved in Opiate Dependence: A Microdialysis Study, The Journal of Neuroscience 22 (2002) 1034–1041. https://doi.org/10.1523/JNEUROSCI.22-03-01034.2002.

[10] O.S. Mabrouk, Q. Li, P. Song, R.T. Kennedy, Microdialysis and Mass Spectrometric Monitoring of Dopamine and Enkephalins in the Globus Pallidus Reveal Reciprocal Interactions that Regulate Movement, J Neurochem 118 (2011) 24. https://doi.org/10.1111/J.1471-4159.2011.07293.X.

[11] Q. Li, Jon-Kar Zubieta, R.T. Kennedy, Practical Aspects of in Vivo Detection of Neuropeptides by Microdialysis Coupled Off-Line to Capillary LC with Multi-stage MS, Anal Chem 81 (2009) 2242. https://doi.org/10.1021/AC802391B.

[12] H.M. Baseski, C.J. Watson, N.A. Cellar, J.G. Shackman, R.T. Kennedy, Capillary liquid chromatography with MS3 for the determination of enkephalins in microdialysis samples from the striatum of anesthetized and freely-moving rats, Journal of Mass Spectrometry 40 (2005) 146–153. https://doi.org/10.1002/jms.733.

[13] R. Al-Hasani, J.-M.T. Wong, O.S. Mabrouk, J.G. McCall, G.P. Schmitz, K.A. Porter-Stransky, B.J. Aragona, R.T. Kennedy, M.R. Bruchas, In vivo detection of optically-evoked opioid peptide release, Elife 7 (2018). https://doi.org/10.7554/eLife.36520.

[14] R. Al-Hasani, J.G. McCall, G. Shin, A.M. Gomez, G.P. Schmitz, J.M. Bernardi, C.-O. Pyo, S. Il Park, C.M. Marcinkiewcz, N.A. Crowley, M.J. Krashes, B.B. Lowell, T.L. Kash, J.A. Rogers, M.R. Bruchas, Distinct Subpopulations of Nucleus Accumbens Dynorphin Neurons Drive Aversion and Reward., Neuron 87 (2015) 1063–77. https://doi.org/10.1016/j.neuron.2015.08.019.

[15] B.E. Pirino, M.B. Spodnick, A.T. Gargiulo, G.R. Curtis, J.R. Barson, A.N. Karkhanis, Kappa-opioid receptor-dependent changes in dopamine and anxiety-like or approach-avoidance behavior occur differentially across the nucleus accumbens shell rostro-caudal axis, Neuropharmacology 181 (2020). https://doi.org/10.1016/J.NEUROPHARM.2020.108341.

[16] B.H. Trieu, B.C. Remmers, C. Toddes, D.D. Brandner, E.M. Lefevre, A. Kocharian, C.L. Retzlaff, R.M. Dick, M.A. Mashal, E.A. Gauthier, W. Xie, Y. Zhang, S.S. More, P.E. Rothwell, Angiotensin-converting enzyme gates brain circuit–specific plasticity via an endogenous opioid, Science (1979) 375 (2022) 1177–1182. https://doi.org/10.1126/SCIENCE.ABL5130/SUPPL_FILE/SCIENCE.ABL5130_DATA_S1.ZIP.

[17] S.M. Reynolds, K.C. Berridge, Positive and negative motivation in nucleus accumbens shell: bivalent rostrocaudal gradients for GABA-elicited eating, taste “liking”/"disliking" reactions, place preference/avoidance, and fear, J Neurosci 22 (2002) 7308–7320. https://doi.org/10.1523/JNEUROSCI.22-16-07308.2002.

[18] D.C. Castro, M.R. Bruchas, A Motivational and Neuropeptidergic Hub: Anatomical and Functional Diversity within the Nucleus Accumbens Shell, Neuron 102 (2019) 529–552. https://doi.org/10.1016/J.NEURON.2019.03.003.

[19] A.G. Schindler, D.I. Messinger, J.S. Smith, H. Shankar, R.M. Gustin, S.S. Schattauer, J.C. Lemos, N.W. Chavkin, C.E. Hagan, J.F. Neumaier, C. Chavkin, Stress produces aversion and potentiates cocaine reward by releasing endogenous dynorphins in the ventral striatum to locally stimulate serotonin reuptake, J Neurosci 32 (2012) 17582–17596. https://doi.org/10.1523/JNEUROSCI.3220-12.2012.

[20] D.C. Castro, K.C. Berridge, Opioid Hedonic Hotspot in Nucleus Accumbens Shell: Mu, Delta, and Kappa Maps for Enhancement of Sweetness “Liking” and “Wanting,” Journal of Neuroscience 34 (2014) 4239–4250. https://doi.org/10.1523/JNEUROSCI.4458-13.2014.

[21] J.J. Pesavento, B.A. Garcia, J.A. Streeky, N.L. Kelleher, C.A. Mizzen, Mild performic acid oxidation enhances chromatographic and top down mass spectrometric analyses of histones, Mol Cell Proteomics 6 (2007) 1510–1526. https://doi.org/10.1074/MCP.M600404-MCP200.

[22] S.A. Carr, S.E. Abbatiello, B.L. Ackermann, C. Borchers, B. Domon, E.W. Deutsch, R.P. Grant, A.N. Hoofnagle, R. Hüttenhain, J.M. Koomen, D.C. Liebler, T. Liu, B. MacLean, D.R. Mani, E. Mansfield, H. Neubert, A.G. Paulovich, L. Reiter, O. Vitek, R. Aebersold, L. Anderson, R. Bethem, J. Blonder, E. Boja, J. Botelho, M. Boyne, R.A. Bradshaw, A.L. Burlingame, D. Chan, H. Keshishian, E. Kuhn, C. Kinsinger, J.S.H. Lee, S.W. Lee, R. Moritz, J. Oses-Prieto, N. Rifai, J. Ritchie, H. Rodriguez, P.R. Srinivas, R.R. Townsend, J. van Eyk, G. Whiteley, A. Wiita, S. Weintraub, Targeted peptide measurements in biology and medicine: Best practices for mass spectrometry-based assay development using a fit-for-purpose approach, Molecular and Cellular Proteomics 13 (2014) 907–917. https://doi.org/10.1074/MCP.M113.036095/ATTACHMENT/D53FF2E2-A6B1-4AAD-BC0D-B7F9E6821120/MMC1.PDF.

[23] A.G. Difeliceantonio, O.S. Mabrouk, R.T. Kennedy, K.C. Berridge, Enkephalin surges in dorsal neostriatum as a signal to eat, Current Biology 22 (2012) 1918–1924. https://doi.org/10.1016/J.CUB.2012.08.014.

[24] T.L. Ripley, J. Jaworski, P.K. Randall, R.A. Gonzales, Repeated perfusion with elevated potassium in in vivo microdialysis - A method for detecting small changes in extracellular dopamine, J Neurosci Methods 78 (1997) 7–14. https://doi.org/10.1016/S0165-0270(97)00129-5.

[25] M. Comb, P.H. Seeburg, J. Adelman, L. Eiden, E. Herbert, Primary structure of the human Met- And Leu-enkephalin precursor and its mRNA, Nature 295 (1982) 663–666. https://doi.org/10.1038/295663a0.

[26] J. HUGHES, H.W. KOSTERLITZ, T.W. SMITH, THE DISTRIBUTION OF METHIONINE-ENKEPHALIN AND LEUCINE-ENKEPHALIN IN THE BRAIN AND PERIPHERAL TISSUES, Br J Pharmacol 120 (1997) 428–436. https://doi.org/10.1111/j.1476-5381.1997.tb06829.x.

[27] G. Henderson, J. Hughes, H.W. Kosterlitz, In vitro release of Leu- and Met-enkephalin from the corpus striatum, Nature 1978 271:5646 271 (1978) 677–679. https://doi.org/10.1038/271677a0.

[28] T. Yoshimasa, K. Nakao, H. Ohtsuki, S. Li, H. Imura, Methionine-enkephalin and leucine-enkephalin in human sympathoadrenal system and pheochromocytoma, Journal of Clinical Investigation 69 (1982) 643–650. https://doi.org/10.1172/JCI110491.

[29] J.A. Mansi, S. Laforest, G. Drolet, Effect of stress exposure on the activation pattern of enkephalin-containing perikarya in the rat ventral medulla, J Neurochem 74 (2000) 2568–2575. https://doi.org/10.1046/J.1471-4159.2000.0742568.X.

[30] E.C. Dumont, R. Kinkead, J.F. Trottier, I. Gosselin, G. Drolet, Effect of chronic psychogenic stress exposure on enkephalin neuronal activity and expression in the rat hypothalamic paraventricular nucleus, J Neurochem 75 (2000) 2200–2211. https://doi.org/10.1046/J.1471-4159.2000.0752200.X.

[31] S. Ceccatelli, C. Orazzo, Effect of different types of stressors on peptide messenger ribonucleic acids in the hypothalamic paraventricular nucleus, Acta Endocrinol (Copenh) 128 (1993) 485–492. https://doi.org/10.1530/ACTA.0.1280485.

[32] R.J. Valentino, E. van Bockstaele, Endogenous opioids: The downside of opposing stress, Neurobiol Stress 1 (2015) 23–32. https://doi.org/10.1016/J.YNSTR.2014.09.006.

[33] I. Melo, E. Drews, A. Zimmer, A. Bilkei-Gorzo, Enkephalin knockout male mice are resistant to chronic mild stress, Genes Brain Behav 13 (2014) 550–558. https://doi.org/10.1111/GBB.12139.

[34] A. Bilkei-Gorzo, I. Racz, K. Michel, D. Mauer, A. Zimmer, D. Klingmüller, A. Zimmer, Control of hormonal stress reactivity by the endogenous opioid system, Psychoneuroendocrinology 33 (2008) 425–436. https://doi.org/10.1016/J.PSYNEUEN.2007.12.010.

[35] H. Nam, R. Chandra, T.C. Francis, C. Dias, J.F. Cheer, M.K. Lobo, Reduced nucleus accumbens enkephalins underlie vulnerability to social defeat stress, Neuropsychopharmacology 44 (2019) 1876–1885. https://doi.org/10.1038/s41386-019-0422-8.

[36] J.W. de Jong, S.A. Afjei, I. Pollak Dorocic, J.R. Peck, C. Liu, C.K. Kim, L. Tian, K. Deisseroth, S. Lammel, A Neural Circuit Mechanism for Encoding Aversive Stimuli in the Mesolimbic Dopamine System, Neuron 101 (2019) 133-151.e7. https://doi.org/10.1016/J.NEURON.2018.11.005.

[37] R. Apfelbach, C.D. Blanchard, R.J. Blanchard, R.A. Hayes, I.S. McGregor, The effects of predator odors in mammalian prey species: A review of field and laboratory studies, Neurosci Biobehav Rev 29 (2005) 1123–1144. https://doi.org/10.1016/J.NEUBIOREV.2005.05.005.

[38] T. Endres, M. Fendt, Aversion- Vs fear-inducing properties of 2,4,5-trimethyl-3-thiazoline, a component of fox odor, in comparison with those of butyric acid, Journal of Experimental Biology 212 (2009) 2324–2327. https://doi.org/10.1242/jeb.028498.

[39] V. Farmer-Dougan, S. Chandrashekar, D. Stutzman, K. Bradham, J.D. Dougan, Fox urine as an aversive stimulus: modification of a passive avoidance task, J Gen Psychol 132 (2005) 313–320. https://doi.org/10.3200/GENP.132.3.313-320.

[40] A.L.O. Hebb, R.M. Zacharko, M. Gauthier, F. Trudel, S. Laforest, G. Drolet, Brief exposure to predator odor and resultant anxiety enhances mesocorticolimbic activity and enkephalin expression in CD-1 mice, European Journal of Neuroscience 20 (2004) 2415–2429. https://doi.org/10.1111/j.1460-9568.2004.03704.x.

[41] A. Asok, L.W. Ayers, B. Awoyemi, J. Schulkin, J.B. Rosen, Immediate early gene and neuropeptide expression following exposure to the predator odor 2,5-dihydro-2,4,5-trimethylthiazoline (TMT), Behavioural Brain Research 248 (2013) 85–93. https://doi.org/10.1016/J.BBR.2013.03.047.

[42] A.A. Legaria, B.A. Matikainen-Ankney, B. Yang, B. Ahanonu, J.A. Licholai, J.G. Parker, A. v. Kravitz, Fiber photometry in striatum reflects primarily nonsomatic changes in calcium, Nature Neuroscience 2022 25:9 25 (2022) 1124–1128. https://doi.org/10.1038/s41593-022-01152-z.

[43] P. Bérubé, J.F. Poulin, S. Laforest, G. Drolet, Enkephalin Knockdown in the Basolateral Amygdala Reproduces Vulnerable Anxiety-Like Responses to Chronic Unpredictable Stress, Neuropsychopharmacology 2014 39:5 39 (2013) 1159–1168. https://doi.org/10.1038/npp.2013.316.

[44] P. Bérubé, S. Laforest, S. Bhatnagar, G. Drolet, Enkephalin and dynorphin mRNA expression are associated with resilience or vulnerability to chronic social defeat stress, Physiol Behav 122 (2013) 237–245. https://doi.org/10.1016/J.PHYSBEH.2013.04.009.

[45] M.A. Rosei, C. Blarzino, C. Foppoli, R. Coccia, C. De Marco, The peroxidase-catalyzed oxidation of enkephalins, Biochem Biophys Res Commun 179 (1991) 147–152. https://doi.org/10.1016/0006-291X(91)91347-F.

[46] A. Finn, G. Ågren, P. Bjellerup, I. Vedin, T. Lundeberg, Production and characterization of antibodies for the specific determination of the opioid peptide Met5-Enkephalin-Arg6-Phe7, Scand J Clin Lab Invest 64 (2004) 49–56. https://doi.org/10.1080/00365510410004119.

[47] H.K. Al-Hakeim, S. Zeki Al-Fadhel, A.H. Al-Dujaili, M. Maes, In major depression, increased kappa and mu opioid receptor levels are associated with immune activation, Acta Neuropsychiatr 32 (2020) 99–108. https://doi.org/10.1017/NEU.2019.47.

[48] Plasma met-enkephalin, beta-endorphin and leu-enkephalin levels in human hepatic encephalopathy, (n.d.). https://apps.who.int/iris/handle/10665/117248 (accessed May 10, 2023).

[49] S.M. Conway, M.O. Mikati, R. Al-Hasani, Challenges and new opportunities for detecting endogenous opioid peptides in reward, Addiction Neuroscience 2 (2022) 100016. https://doi.org/10.1016/j.addicn.2022.100016.

[50] A.L.O. Hebb, R.M. Zacharko, M. Gauthier, F. Trudel, S. Laforest, G. Drolet, Brief exposure to predator odor and resultant anxiety enhances mesocorticolimbic activity and enkephalin expression in CD-1 mice, European Journal of Neuroscience 20 (2004) 2415–2429. https://doi.org/10.1111/j.1460-9568.2004.03704.x.

[51] H. Sundberg, K. Døving, S. Novikov, H. Ursin, A method for studying responses and habituation to odors in rats, Behav Neural Biol 34 (1982) 113–119. https://doi.org/10.1016/S0163-1047(82)91501-1.

[52] A.D. Abraham, S.M. Casello, S.S. Schattauer, B.A. Wong, G.O. Mizuno, K. Mahe, L. Tian, B.B. Land, C. Chavkin, Release of endogenous dynorphin opioids in the prefrontal cortex disrupts cognition, Neuropsychopharmacology 2021 (2021) 1–10. https://doi.org/10.1038/s41386-021-01168-2.

[53] D.C. Castro, C.S. Oswell, E.T. Zhang, C.E. Pedersen, S.C. Piantadosi, M.A. Rossi, A.C. Hunker, A. Guglin, J.A. Morón, L.S. Zweifel, G.D. Stuber, M.R. Bruchas, An endogenous opioid circuit determines state-dependent reward consumption, Nature 2021 598:7882 598 (2021) 646–651. https://doi.org/10.1038/s41586-021-04013-0.

[54] B. MacLean, D.M. Tomazela, N. Shulman, M. Chambers, G.L. Finney, B. Frewen, R. Kern, D.L. Tabb, D.C. Liebler, M.J. MacCoss, Skyline: an open source document editor for creating and analyzing targeted proteomics experiments, Bioinformatics 26 (2010) 966–968. https://doi.org/10.1093/BIOINFORMATICS/BTQ054.

[55] V.N. Sherathiya, M.D. Schaid, J.L. Seiler, G.C. Lopez, T.N. Lerner, GuPPy, a Python toolbox for the analysis of fiber photometry data, Scientific Reports 2021 11:1 11 (2021) 1–9. https://doi.org/10.1038/s41598-021-03626-9.